Stored Energy Evaluation for High Strength Dual-Phase Steels with Different Pre-annealing Conditions

Yingjie Wu[1], Juha Uusitalo[2] and Anthony J. DeArdo[1,2*]

[1] Department of Mechanical Engineering and Materials Science, Basic Metals Processing Research Institute, Swanson School of Engineering, University of Pittsburgh, 636 Benedum Hall, 3700 O'Hara Street, Pittsburgh, PA 15261, USA.

[2] Centre for Advanced Steels Research, Materials Engineering Laboratory, Department of Mechanical Engineering, P.O Box 4200, FI-90014 University of Oulu, Oulu, Finland.

The email address of corresponding author: Anthony J. DeArdo*: deardo@pitt.edu

ABSTRACT

The purpose of this study was to determine the stored energy of dual-phase (DP) steels after hot rolling, coiling and cold reduction using electron backscattered diffraction (EBSD) analysis. Three methods for stored energy evaluation were examined and compared: the sub-grain boundary, image quality (IQ) method and kernel average misorientation (KAM) methods. The results demonstrated that the sub-grain method, in which stored energy was calculated as a function of subgrain boundary misorientations and total sub-grain boundary length, can provide more accurate stored energy values, since cold work was responsible for forming numerous dislocation structures such as shear bands, cells and cell walls. As expected, the steels with the combination of a low coiling temperature of 580ºC and 60% cold reduction had the highest stored energy values.

Keywords: Stored energy, dual-phase steels, electron backscattered diffraction (EBSD), dislocation structures, image quality (IQ), kernel average misorientation (KAM)

I. INTRODUCTION

Advanced high strength steels (AHSSs) are widely investigated because they exhibit a good combination of high strength and adequate ductility to reach the requirements of lowering carbon dioxide emissions, reducing weight, increasing fuel efficiency and improving safety. AHSSs are multi-phase steels which combine ductile ferrite with controlled amounts of fresh martensite, tempered martensite, bainite and/ or retained austenite in order to achieve the strength-formability-crash worthiness required. Dual-phase (DP) steels are a good representative of

AHSSs, whose microstructures are characterized by a ferrite matrix and isolated martensite islands [1,2]. Also, dual-phase steels have the mechanical properties of high ultimate tensile strength (UTS), continuous yielding, low yield strength (YS), low yield to tensile strength ratio (YS/UTS), high work hardening ratio (n) and reasonable ductility (both total elongation (TE) and shear-edge ductility) [3]. By design, the high strengths permit the use of thinner gauges, often below 1 mm in cold rolled gauges, to reduce vehicle mass. These thin gauges present a problem of corrosion penetration, especially in halide-rich environments. This problem is alleviated through the use of coatings such as Zn-based or Al-based systems, where the coating is applied by hot dipping in suitable baths after intercritical annealing. Since the continuous hot dipped galvanizing line (CGL) is, in fact, a series of non-equilibrium heat treatments (annealing of the cold rolled ferrite, formation of austenite during intercritical annealing, decomposition of austenite upon cooling) intended to alter the metallurgical microstructure, there has been a large literature published on various aspects of the process [4–8].

After melting, refining and solidification, further processing of solid DP steels consists of hot rolling, cold rolling, intercritical annealing followed by hot dipping in a Zn bath of proper composition (Zn-10%Al) and temperature (near 460ºC [733K]). Stored energy, associated with the lattice defects, mainly dislocations, results from the cumulative effects of the transformation strains associated with the decomposition of austenite during the coiling of the hot rolled hot band and later by the plastic deformation in cold rolling. Since plastic deformation can affect both the thermodynamics and kinetics of annealing and transformation, numerous studies have been performed to measure the amount of stored energy in steels as they enter the hot dipped galvanizing line.

Before transmission electron microscopy (TEM) was applied in the field of physical metallurgy in the early 1950s, attempts had already been made to observe the existence of dislocations and their arrangements, using surface methods such as etch pitting, via optical microscopes. Vogel et al [9] first observed the etch pits, revealing the existence of edge dislocations in the vicinity of the grain boundary areas between two germanium crystals, after chemical etching. Later, Hibbard and Dunne used etch pits to clearly show the progress of polygonization during the annealing of iron-silicon single crystals [10].

These earlier researches endeavored to describe the importance of stored energy. Later approaches involved calorimetry. Leach et al [11] first used the calorimetric method to measure the stored energy of deformed Au-Ag alloys. Since differential microcalorimeters were invented by Watson and O'Neill [12], differential scanning calorimetry (DSC) has been developed and applied to measuring the stored energy of materials [11,13–15]. In the DSC method, the deformed specimens are annealed [13] and the elastic strain energy caused by the dislocations accompanying plastic deformation is released as heat and measured during recovery and recrystallization [14]. X-ray diffraction (XRD) techniques have also contributed to determining the structures of cold worked materials since the 1930s, and XRD line broadening has been ascribed to internal strain caused by plastic deformation. Paterson [16] used the line broadening method to determine the internal strains and combined Stibitz's [17] formula to calculate the stored energy of deformed calcite. Kallend and Huang [18] improved the XRD line broadening method to evaluate the general orientation dependent stored energy of 50% cold rolled copper and also reported that stored energy was increased with the increasing of the Taylor factor of the grains in the polycrystals studied. Rajmohan et al. [19] started to use a neutron diffraction line broadening method instead of XRD line broadening to calculate the stored energy of 80% cold rolled interstitial free (IF) steels, since neutrons can penetrate through the bulk materials with a large diffraction volume and not be affected by the surface conditions of samples, giving a more accurate stored energy value. Dillamore et al. [20] found that sub-grain growth dominated the grain-boundary nucleation in the early stage of recrystallization. Also, in their work, stored energy was calculated as a function of misorientations of sub-grain boundaries, the using Shockley-Read low angle grain boundary (LAGB) energy formula [21,22]. This sub-grain method has been subsequently developed and applied to numerous materials (i.e., cold rolled oxygen free electrolytic (OFE) copper [23], low carbon steels [24], IF steels [15], Fe-48%Ni alloys [25] and Ti or Nb bearing high strength low alloy (HSLA) steels [26]), since sub-grain boundary misorientations can be determined and classified automatically from EBSD data. Later, Image Quality (IQ) data were generated from electron backscattered diffraction (EBSD) data, and is used to indicate the quality of a diffraction pattern. From the Hough Transform, IQ is defined as the average height of the intensity peaks which are converted from Kikuchi bands [27]. The lattice defects, especially dislocations, introduced by phase transformation or plastic deformation can cause the

imperfection of crystalline lattices [27–29]. In Choi and Yin's research [24], an association was found between the stored energy of cold rolled low carbon steels and IQ values.

Kernel average misorientation (KAM) is also another approach for characterizing the local misorientation of deformed crystalline lattices. It is defined as the average misorientation of a single point with regard to its neighbors within a kernel [28]. During plastic deformation, statistically stored dislocations (SSDs) accumulate by random trapping, whereas geometrically necessary dislocations (GNDs) are stored, allowing for the compatible deformations, which are related to the gradients of deformations [30]. Calcagnotto et al. [31] suggested that geometrically necessary dislocation density (ρ_{GND}) could be calculated from KAM values. Therefore, stored energy can be expressed as the dislocation energy [32] with respect to EBSD-KAM.

In this current study, the stored energy values for DP steels entering the CGL with different initial pre-annealing conditions were estimated from EBSD data, using the sub-grain, IQ and KAM methods. Meanwhile, the effects of pre-annealing conditions (i.e., coiling temperature and cold reduction) on stored energy were also investigated.

II. EXPERIMENTAL PROCEDURE

A. *Materials*

The chemical compositions of candidate DP steels used in this investigation are given in Table I. Table I lists two compositional variations (aluminum & vanadium), the base composition and designations used in this paper. The first digit of the designation represents the aluminum level (0.04 wt.% Al was labeled by L, 0.4 wt.% by M and 0.8 wt.% by H), and the second digit denotes the vanadium content (0.06 wt.% V was denoted by L and 0.12 wt.% by H). Later, a third digit will be added to indicate the coiling temperature (H for high and L for low temperatures)

Table I The chemical compositions (wt. %) of candidate DP steels

Designation	Al (wt.%)	V (wt.%)	Base
LL	0.04	0.06	0.15C-2.0Mn-0.01P-0.003S-0.4Si-0.02Cu-0.01Ni-0.5Cr-0.005Mo-0.004Ti-0.005N
LH	0.04	0.12	
ML	0.4	0.06	
MH	0.4	0.12	

HL	0.8	0.06

B. *Processing*

The whole processing of the laboratory vacuum induction-melted 45 kg ingots used in this research consisted of hot rolling, surface grinding and cold rolling (Fig. 1). For rough rolling, the ingots were reheated to 1250ºC (1523K), followed by rough rolling to 25 mm with several passes. In terms of finishing rolling, the steels were again reheated to 1250ºC (1523K) and hot rolled with 5 passes of reductions, each of which was ~ 27.5%, to the final thickness of 5 mm, with the finishing rolling temperature (FRT) of 920ºC (1193K). Subsequently, the steels were water sprayed to the coiling temperature of 677ºC (950K) or 580ºC (853K) at a cooling rate of -30ºC s^{-1} (-30K s^{-1}), followed by controlled cooling to room temperature at -30ºC h^{-1} (-30K h^{-1}). The surface grinding of the hot rolled steels removed the oxide layers and impurities on the surface of hot band coils, and the desired surfaces were obtained with the thickness of 3 mm. After surface grinding, the steels were 60% cold rolled to the final thickness of 1.2 mm. This processing led to a series of steel conditions where each steel/condition was labelled with three letters, one for the Al level, one for the V level and the third for the coiling temperature (either H = 677ºC [950K] or L = 580ºC [853K]).

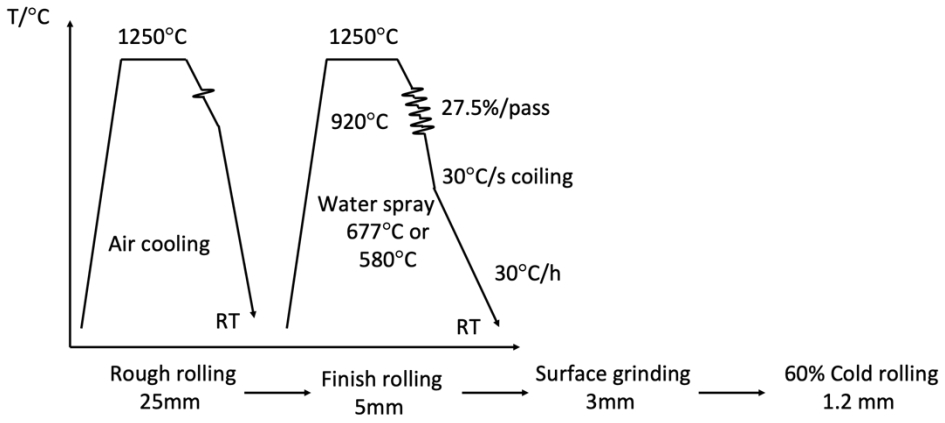

Figure 1-The schematic process of the steels used in this study consisting of hot rolling, surface grinding and cold rolling.

C. *Microstructure Characterization*

The samples were sectioned, and the rolling surface of each sample was ground with 600~1200 grit SiC abrasive grinding papers. After mechanical grinding, the samples were polished by a Buehler VibroMet^{TM} 2 vibration polisher for 45 - 60 min with a 0.05 μm alumina suspension. Then, each sample was etched by a 2% Nital reagent for the observation of OM and the FEI Apreo SEM. In terms of EBSD analysis, the standard metallurgical sample preparation needs to be more careful, in case that the mechanical deformation during surface preparation might introduce defects into the crystalline lattice and complicate the subsequent analysis. Therefore, each sample was vibratory polished for more than 5 hr. As long as the surface of each sample is completely flat, polishing steps can be stopped. Also, in this case, samples were not allowed to be etched, since the topologies of different phases would block the backscattered electrons from reaching the EBSD detector. The electron back scattered diffraction patterns (EBSPs) were generated and collected by the FEI Apreo SEM, equipped with a TEAM^{TM} EBSD analysis system. A voltage of the SEM was 20kV as well as a spot size of 15 or current of 13 nA. was used in the data acquisition. The parameters of EBSD mapping were chosen according to the specific information of the samples. Normally, the step size was 0.1 μm with a magnification of 1000×. The dimension of an EBSD map was 60 μm × 60 μm and the mapping grid was chosen as a square grid.

III. Stored Energy (SE) Evaluation

A. *Sub-Grain Method*

The stored energy can be described as a function of misorientation and the internal strain energy can be stored in the dislocations in the sub-grain boundaries [20]. So, the energy stored in sub-grain boundaries (SE_d) can be expressed as Eq. 1 [33].

$$SE_d = \frac{k\gamma_s}{d} \tag{1}$$

where, k is the geometric constant (k=3 [33]), γ_s is the sub-grain boundary energy and d is the average sub-grain size. This equation can be rewritten as Eq. 2

$$\frac{SE_d}{\gamma_m} = \frac{k}{d}\left(\frac{\gamma_s}{\gamma_m}\right) \tag{2}$$

where, γ_m is the maximum grain boundary energy. γ_s can be determined by Shockley-Read LAGB energy formula [21,22], shown in Eqs. 3 and 4 [22,24],

$$\gamma_s = \gamma_m \frac{\theta}{\theta_m}\left[1 - \ln\left(\frac{\theta}{\theta_m}\right)\right], \qquad \text{if } \theta < \theta_m \tag{3}$$

$$\gamma_s = \gamma_m, \text{ if } \theta \geq \theta_m \tag{4}$$

where, θ_m is the limit for the low angle grain boundary misorientation ($\theta_m = 15^o$). γ_m is the special boundary energy for HAGBs (γ_m=7.56 J m^{-2} [26]). Note: γ_s = 3.95 J m^{-2} when $\theta = 3^o$, the definition of sub-grain boundary misorientation using dislocation models [34].

B. *IQ Method*

IQ is an index for depicting the quality of diffraction patterns constructed from EBSD and it is defined as the average height of intensity peaks converted from Kikuchi bands, seen in Eq. 5 [27],

$$IQ = \frac{1}{N}\sum_{i=1}^{N} H_i(\rho_i,\theta_i) \tag{5}$$

where, N is the number of the peaks; H_i is the height of the ith peaks; and (ρ_i and θ_i) are Hough parameters of the ith peak, illustrating the location of the ith peak in the Hough Transform. The length of intensity peak was reported to be related to the quality of diffraction patterns or the perfection level of diffracted crystalline lattices [23,24,35]. The more dislocations are introduced by plastic deformations, the more severe imperfection of diffracted crystalline lattices is, resulting in smaller IQ values. Thus, stored energy can be linked to reconstructed IQ values, as shown in Eq. 6 [24],

$$SE_d \propto IQ = \left(1 - \frac{IQ_i - IQ_{min}}{IQ_{max} - IQ_{min}}\right) \times 10 \tag{6}$$

where, IQ_i is the IQ value of the ith diffracted site; IQ_{min} and IQ_{max} are the minimum and maximum IQ values of the scanning set for each sample. The IQ method can depict the effects of cold deformations on subsequent recovery and recrystallization during annealing, but it cannot quantitatively estimate stored energy itself. However, it is a method for comparing elastic stored energy on a local level for different locations.

C. *KAM Method*

In the EBSD analysis, local misorientation denotes the strain distribution of bulk materials [25,31], and KAM is one of the most useful approaches. In this case, for a given spot in the kernel for hexagonal grids, its local misorientation is calculated by averaging the misorientations of all the spots within a kernel or of the spots in the perimeter area of a kernel. The average KAM values can be determined by Eq. 7 [25],

$$\mathrm{KAM} = \frac{1}{\mathrm{N}}\sum_{\mathrm{i=1}}^{\mathrm{N}} \theta_{\mathrm{i}} \tag{7}$$

where, N is the number of spots within a kernel and θ_i represents the misorientation of a spot within the kernel with represent to the given spot.

In 1970， Ashby [30] put forward the concepts of statistically stored dislocations (SSDs) and geometrically necessary dislocations (GNDs) after nonhomogeneous plastic deformation. The distinction between these two concepts were examined, determined and explained by numerous researchers[31,36–39]. SSDs evolve from random trapping during uniform plastic deformation [30], and these dislocations do not cause significantly lattice rotation, thereby making net burgers vectors equivalent to zero [37]. In contrast, GNDs are stored associated with plastic strain gradients during nonhomogeneous plastic deformation [30], which results in geometrical constrains to lattice crystals [38]. The geometrically necessary dislocation density (ρ_{GND}) can be quantitively calculated from local misorientation, since ρ_{GND} is linearly related to the gradient of plastic deformation, causing the curvature of the crystalline lattice. EBSD-KAM is one of the methods used for predicting local misorientation, so ρ_{GND} can be expressed as a function of KAM values. The relationship between KAM and ρ_{GND} can be shown in Eq. 8 [25,31] ,

$$\rho_{\mathrm{GND}} = \frac{\alpha \mathrm{KAM}}{\mathrm{Xb}} \tag{8}$$

where, α is a constant related to grain boundary types: α=2 for tilt boundaries, α=4 for twist boundaries and α=3 for mixed boundaries [25] (only the simplest tilt boundaries are taken into consideration in this research). KAM values in degrees should be converted into the ones in radians, X is the unit length (X=nd, n is the kernel size (n=2) and d is the step size (d=100nm)). b

is the Burgers vector, which for iron is ($|\mathbf{b}_{<111>}|=\frac{\sqrt{3}}{2}a$=0.248 nm). In terms of the KAM calculation, the threshold of misorientation is chosen between 0 – 2º.

Most stored energy can be accumulated into the sub-grain boundaries, especially in alloys of high stacking fault energy. It can be calculated by Eq. 9 [32],

$$SE_d = \frac{1}{2} G \rho_{GND} b^2 \quad (9)$$

where, G is shear modulus (G=82GPa [40]).

D. *High Angle Grain Boundary Energy*

The other part of stored energy comes from elongated ferrite grain boundaries or high angle grain boundaries (HAGBs) after plastic deformation. This part of stored energy can be calculated by Eq. 10 [26],

$$SE_{HAGB} = 7.56 \times S_V \times 10^{-5} \quad (10)$$

where, S_V is the interfacial surface area of sub-grain boundary per unit volume. For equiaxed HAGBs (such as hot rolled ferritic steels finish rolled at high temperatures), S_V can be expressed by Eq. 11 [41],

$$S_V = 2N_L \quad (11)$$

where, N_L is the intercept number per unit length. For elongated HAGBs (such as cold rolled ferritic steels), S_V can be illustrated by Eq. 12 [41],

$$S_V = 0.429 (N_L)_{\parallel} + 1.571 (N_L)_{\perp} \quad (12)$$

where, $(N_L)_{\parallel}$ and $(N_L)_{\perp}$ are the intercept umbers per unit length along RD and TD, respectively. The total stored energy (SE_{tot}) should then be the energy contributed from the sub-grain boundary energy (SE_d) plus the HAGB energy (SE_{HAGB}), which is expressed by Eq. 13,

$$SE_{tot} = SE_d + SE_{HAGB} \quad (13)$$

IV. Results

A. *Initial Microstructures of Hot Band Coils and Cold Rolled Sheets*

The microstructures of hot band coils with a low coiling temperature of 580ºC (853K) are shown in Fig. 2 (a). The microstructures consist of acicular ferrite, polygonal ferrite and pearlite. The microstructures of hot bands coiled at 677ºC (950K), comprising banded polygonal ferrite and pearlite aggregates along the rolling direction (RD), are shown in Fig. 2 (b). The average ferrite grain sizes (d_α), ferrite volume fractions ($fv_{(\alpha)}$) and pearlite percentages ($fv_{(P)}$) of hot band coils in different pre-annealing conditions are listed in Table II. The average ferrite grain sizes vary with Al contents, V levels and coiling temperatures (Fig. 3). (1) Among the three distinct Al contents, the hot band coils containing 0.4 wt.% Al have the finest ferrite grains. (2) The ferrite grains become slightly coarser, as the V level was increased from 0.06 wt.% to 0.12 wt.%. (3) For the low coiling temperature, the average ferrite grain sizes range from 4.4 to 5.7 µm. While, the ferrite grain sizes can reach 9.2 µm, when the coiling temperature reaches 677ºC (950K). The initial ferrite volume fractions of these steels are ~ 60 – 70%.

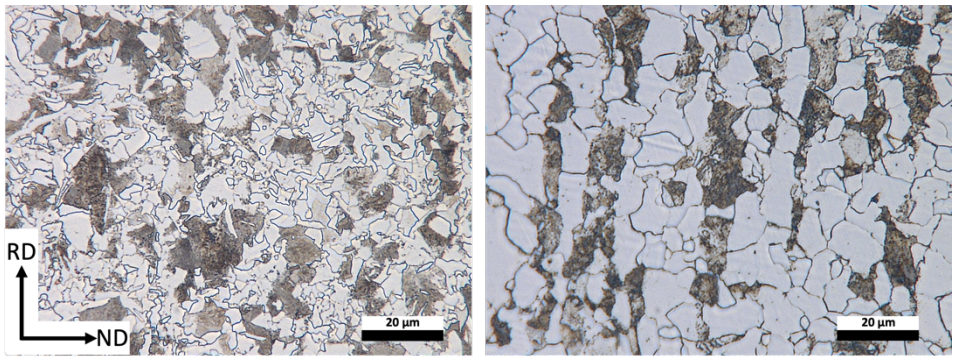

(a) **(b)**

Figure 2-OM micrographs of hot band coils (HB) with two different coiling temperatures: (a) LLL HB (0.04Al-0.06V-CT580ºC [853K]) and (b) LLH HB (0.04Al-0.06V-CT677ºC [950K])

Table II Ferrite grain sizes (d_α), ferrite volume fractions ($fv_{(\alpha)}$) and pearlite volume percentages ($fv_{(P)}$) of hot band coils in different conditions

Designation	d_α (µm)	$fv_{(\alpha)}$ (%)	$fv_{(P)}$ (%)
LLL HB	5.57±3.08	69.3	30.8
LHL HB	5.68±3.47	74.3	25.7

MLL HB	4.44±2.79	61.7	38.3
MHL HB	5.06±3.40	71.1	28.9
HLL HB	5.22±3.34	68.5	31.5
LLH HB	8.70±4.17	71.5	28.5
LHH HB	9.22±4.56	67.7	32.3
MLH HB	6.08±3.58	58.9	41.1
MHH HB	6.71±3.92	65.5	34.5
HLH HB	7.66±3.58	75.9	24.1

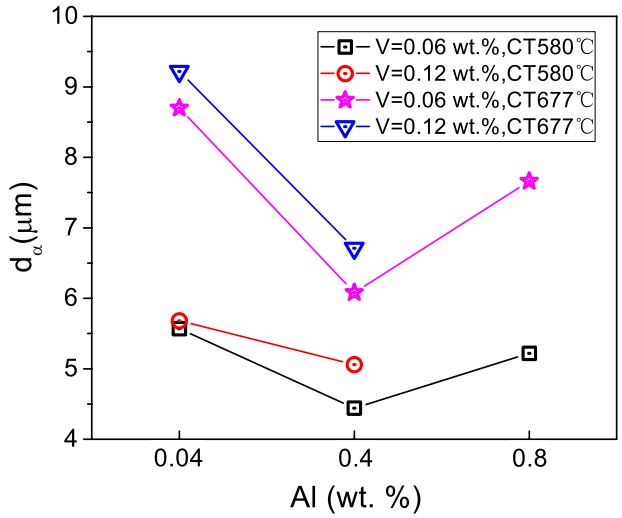

Figure 3-The average ferrite grain sizes of DP hot band coils in different conditions

Fig. 4 shows the OM micrographs of cold rolled steels with two different coiling temperatures. The acicular ferrite, polygonal ferrite and pearlite of cold rolled steel with a low coiling temperatures are deformed along the RD, seen in Fig. 4 (a). The ferrite grains are compacted so tightly that the ferrite grain boundaries are barley observed. Like the microstructures for low temperature coiled and cold rolled steels, the polygonal ferrite and pearlite in the cold rolled steels with a high coiling temperature are also elongated along RD, whereas, the ferrite grain sizes are coarser, shown in Fig. 4 (b).

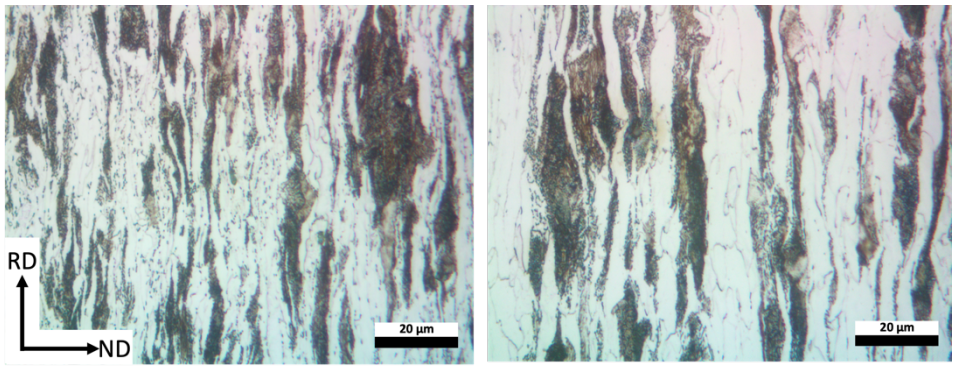

Figure 4-OM micrographs of cold rolled steels (CR) with two different coiling temperatures: (a) LLL CR (0.04Al-0.06V-CT580ºC [853K]) and (b) LLH CR (0.04Al-0.06V-CT677ºC [950K])

B. *EBSD Analyses of Hot Band Coils and Cold Rolled Steel Sheets*

The IQ maps of HLL (0.8%Al-0.06%V-CT580ºC [853K]) hot band coils (HB), HLL cold rolled sheet steels (CR), HLH (0.8%Al-0.06%V-CT677ºC [950K]) HB and HLH CR with black lines showing HAGBs (> 15°), are shown in Figs. 5 (a) to (d). The contrast observed in IQ maps are mainly due to plastic internal strains. The light appearing areas show low internal strains, while darker regions represent high internal strains. For hot band coils, a higher strain contrast is observed in the IQ map of the sample coiled at 580ºC (853K), Fig. 5 (a), compared with that of the sample with a high coiling temperature of 677ºC (950K), Fig. 5 (c). A large number of acicular ferrites (also called low temperate ferrite) form at a low coiling temperature of 580ºC (853K), possessing a “needle-like” grain shape as well as high dislocation densities and causing the imperfection of crystalline lattices, however, polygonal ferrite nucleates at a high coiling temperature (677ºC [950K] in this study) and has an equiaxed grain shape and low dislocation densities with no existence of sub-structures [42]. The difference in dislocation densities of these two types of ferrites results in the apparent strain contrast in Fig. 5 (a). Concerning the cold rolled sheet steels, seen in Figs. 5 (b) and (d), very high dislocation densities were introduced by the 60% cold reduction, the internal strains of cold rolled steels are considerably larger than those of hot band coils. The inverse pole figure (IPF) maps of HLL HB, HL CR, HLH HB and HLH CR are presented in Figs. 5 (e) to (h). A ferrite orientation triangle can be observed in Fig. 5 (e). The KAM maps of HLL HB, HL CR, HLH HB and HLH CR with a kernel misorientation

color code are exhibited in Figs. 5 (i) to (l). Similar to the strain contrast in IQ maps, the color distribution of kernel misorientations in KAM maps provides the local strain distribution of samples [28]. From Calcagnotto et al.'s study [31], geometrically necessary dislocation densities held a positively linear relation with KAM values. Combined with misorientation color code, cold colors (blue and green) show the low misorientations or low ρ_{GND} and warm colors (yellow, orange and red) denote the high misorientations or high internal strains. Thus, the KAM map of the steel with the combination of the low coiling temperature of 580ºC (853K) and 60% cold reduction, in Fig. 5 (j), shows the most intense local strain distribution, compared with those of the steels with the other three pre-annealing conditions.

The SE maps based on the sub-grain method of HLL HB, HLL CR, HLH HB and HLH CR are shown in Figs. 5 (m) to (p). The intensity of red color in SE maps presents the stored energy distribution. The low temperature coiled and 60% cold rolled steel has the highest stored energy distribution, seen in Fig 5 (n). The detailed stored energy calculation based on the sub-grain method will be discussed in the following section.

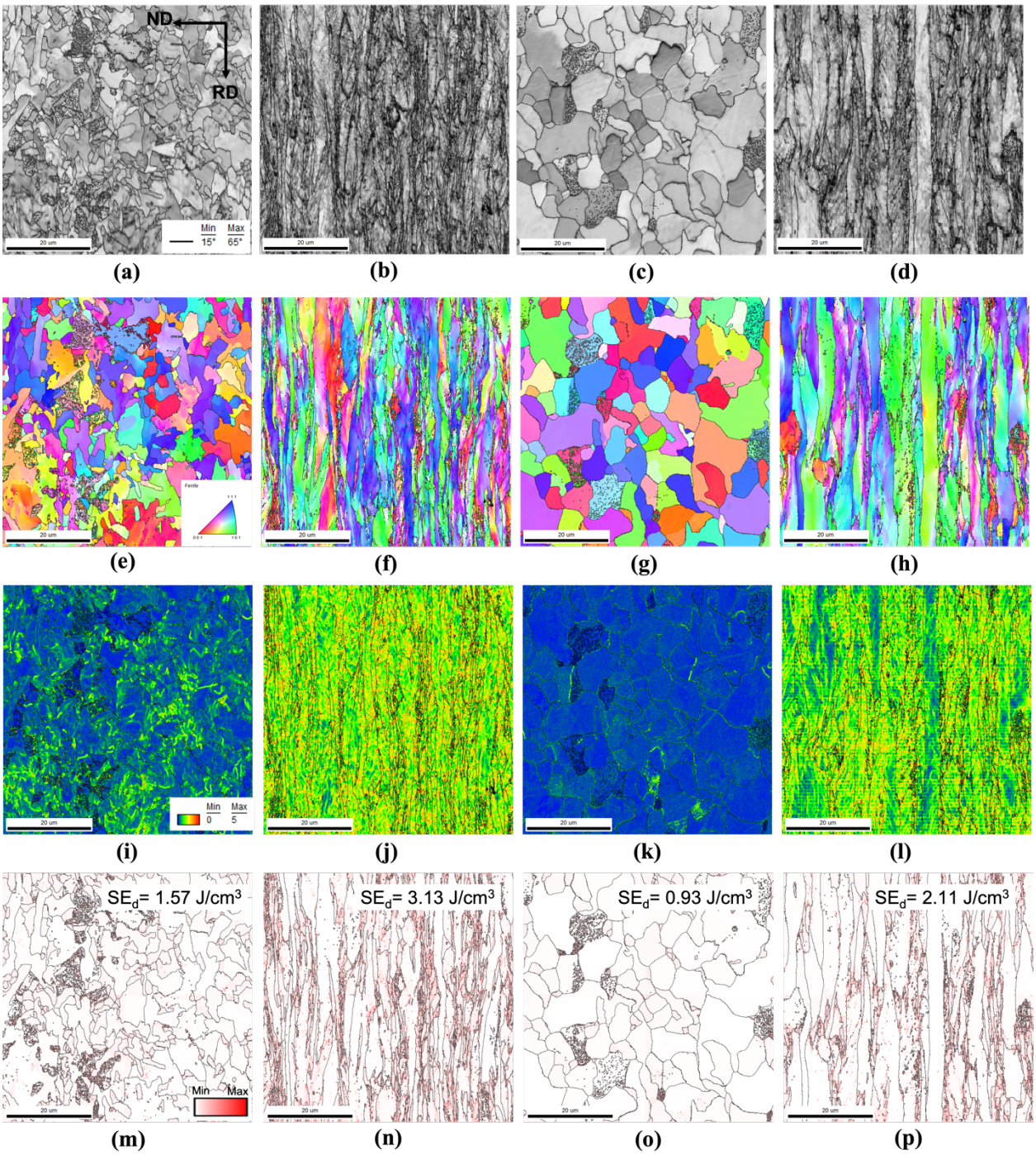

Figure 5-EBSD-IQ maps of (a) HLL (0.8%Al-0.06%V-CT580ºC [853K]) HB, (b) HLL CR, (c) HLH (0.8%Al-0.06%V-CT677ºC [950K]) HB and (d) HLH CR. EBSD-IPF maps of (e) HLL HB, (f) HLL CR, (g) HLH HB and (h) HLH CR. EBSD-KAM maps of (i) HLL HB, (j) HLL CR, (k) HLH HB and (l) HLH CR. EBSD-SE maps, based on the sub-grain method, of (m) HLL HB, (n) HLL CR, (o) HLH HB and (p) HLH CR

C. *Stored Energy Evaluation Based on Sub-Grain Method*

The stored energies calculated by the sub-grain method for hot band coils and cold rolled sheet steels with initial pre-annealing conditions are listed in Table III. In this method, the energy is considered to be stored in sub-grain boundaries [26] formed by the geometrically necessary dislocations, which are introduced by phase transformation or plastic deformation. It should be noted that, for both hot band coils and cold rolled sheets, the coiling temperature can affect the stored energy. From Table III, the stored energy for steels coiled at 580ºC (853K) is larger than that of steels with a high coiling temperature of 677ºC (950K), since the transformation of acicular ferrite leads to high dislocation densities or more sub-grain boundaries [42]. In addition to coiling temperature, the cold reduction also influences stored energy. For example, in terms of sample LLL (0.04%Al-0.06%V-CT580ºC [853K]), the stored energy increases from 1.65 J cm^{-3} to 3.50 J cm^{-3} after 60% cold reduction, since a great amount of cold work was consumed by forming numerous dislocation structures such as cells and shear bands [24]. Also, the stored energy distribution maps, shown in Figs. 5 (m) to (p), are based on the combination of the sub-grain method and EBSD technology. Figs. 5 (m)-(p) present the stored energy distribution maps, using sub-grain method, for steels HL (0.8Al-0.06V) with four pre-annealing conditions: low coiling temperature without cold reduction (Fig. 5 (m)), low coiling temperature with cold reduction (Fig. 5 (n)), high coil temperature without cold reduction (Fig. 5 (o)) and high coiling temperature with cold reduction (Fig. 5 (p)). It must be emphasized that the combination of low coiling temperature of 580ºC [853K] and 60% cold reduction leads to a relatively higher stored energy, providing more driving force for ferrite recovery and recrystallization as well as austenite nucleation and growth during the following intercritical annealing.

Table III SE_d for hot band coils (HB) and cold rolled steels (CR) based on sub-grain method

Designation	SE_d (HB) ($J\ cm^{-3}$)	SE_d (CR) ($J\ cm^{-3}$)	Designation	SE_d (HB) ($J\ cm^{-3}$)	SE_d (CR) ($J\ cm^{-3}$)
LLL	1.65	3.50	LLH	1.06	2.00
LHL	1.33	3.09	LHH	0.96	2.71
MLL	1.45	3.68	MLH	0.79	2.63
MHL	1.36	3.45	MHH	1.08	2.46
HLL	1.57	3.13	HLH	0.93	2.11

D. *Stored Energy Evaluation Based on IQ Method*

Figs. 6 (a) to (d) show the reconstructed IQ distributions of HLL (0.8%Al-0.06%V-CT580ºC [853K]) hot band coils (HB), HLL cold rolled sheet steels (CR), HLH (0.8%Al-0.06%V-CT677ºC [950K]) HB and HLH CR. In previous studies, each IQ value is considered to be linked to the work hardening state of each diffracted site [23]. For example, the microstructures of hot band coils characterized by polygonal ferrite with low internal strains or low dislocation densities normally have high IQ values, however, the cold rolled steels consisting of deformed and elongated ferrite grains have low IQ data [35]. In this research, the reconstructed IQ value for each site was calculated by Eq. 6 and each reconstructed IQ value ranges from 0 to 10. In addition, the reconstructed IQ for each diffracted site has a positively linear relation with its internal strain or dislocation density. The average reconstrued IQ values (IQ_{mean}) for steel HL (0.8%Al-0.06%V) with four initial conditions are also presented in Fig. 6. The results demonstrated that IQ_{mean} (CT580ºC [853K], CR) > IQ_{mean} (CT677ºC [950K], CR) > IQ_{mean} (CT580ºC [853K], HB) > IQ_{mean} (CT677ºC [950K], HB).

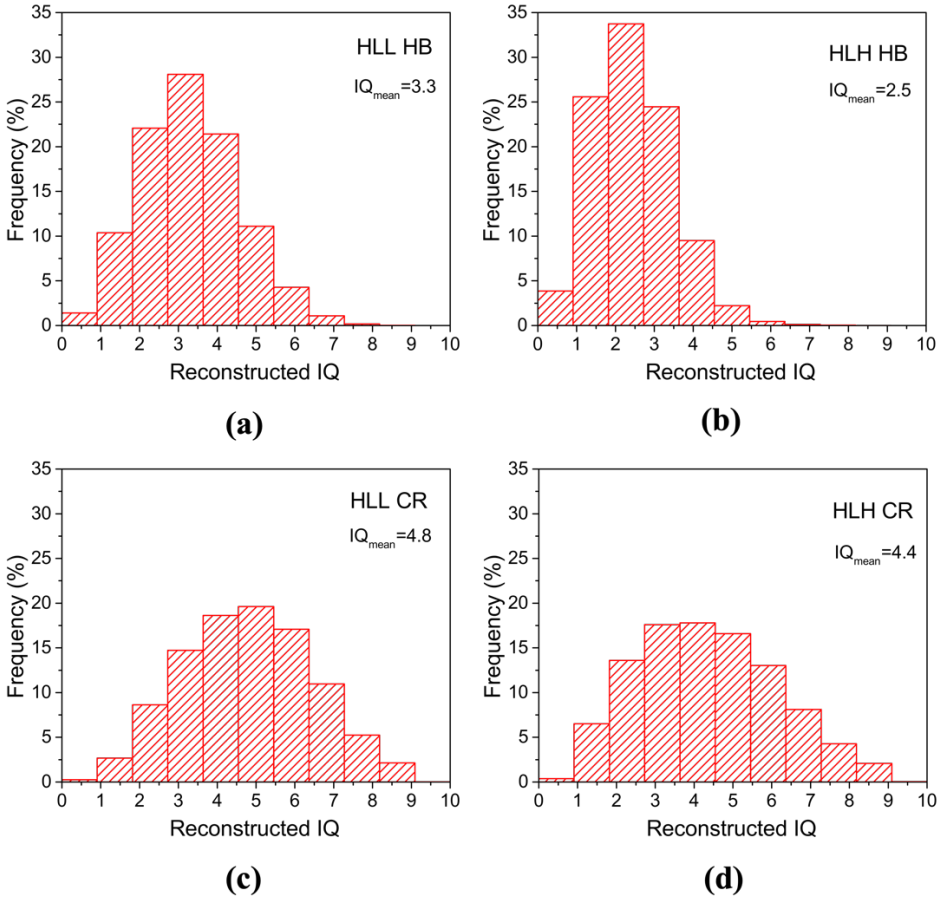

Figure 6-Reconstructed IQ distributions of (a) HLL (0.8%Al-0.06%V-CT580ºC [853K]) HB, (b) HLL CR, (c) HLH (0.8%Al-0.06%V-CT677ºC [950K]) HB and (d) HLH CR.

E. *Stored Energy Evaluation Based on KAM Method*

The KAM values of hot band coils and cold rolled steels with distinct initial conditions are listed in Tables IV and V, respectively. The ρ_{GND} was calculated by Eq. 8 and SE_d was evaluated by Eq. 6 , which are also recorded in Tables IV and V. Similar to the results shown in Table III, the SE_d of steels using the KAM method varies with initial conditions. The SE_d values for steels with low temperature coiling and cold rolled steels are much higher. Also, it seems that chemical compositions may not have an obvious effects on SE_d in this study.

Table IV KAM, ρ_{GND} and SE_d for hot band coils based on KAM method

Designation	KAM (°)	$10^{10} \times \rho_{GND}$ (cm^{-2})	SE_d ($J\ cm^{-3}$)	Designation	KAM (°)	$10^{10} \times \rho_{GND}$ (cm^{-2})	SE_d ($J\ cm^{-3}$)
LLL HB	0.568	4.00	1.01	LLH HB	0.347	2.44	0.62
LHL HB	0.519	3.65	0.92	LHH HB	0.409	2.88	0.73
MLL HB	0.617	4.34	1.09	MLH HB	0.380	2.67	0.67
MHL HB	0.634	4.46	1.12	MHH HB	0.395	2.78	0.70
HLL HB	0.585	4.11	1.04	HLH HB	0.384	2.70	0.68

Table V KAM, ρ_{GND} and SE_d for cold rolled steels based on KAM method

Designation	KAM (°)	$10^{10} \times \rho_{GND}$ (cm^{-2})	SE_d ($J\ cm^{-3}$)	Designation	KAM (°)	$10^{10} \times \rho_{GND}$ (cm^{-2})	SE_d ($J\ cm^{-3}$)
LLL CR	1.302	9.16	2.31	LLH CR	1.146	8.06	2.03
LHL CR	1.289	9.07	2.29	LHH CR	1.223	8.60	2.17
MLL CR	1.288	9.06	2.28	MLH CR	1.220	8.58	2.16
MHL CR	1.315	9.25	2.33	MHH CR	1.203	8.46	2.13
HLL CR	1.202	8.45	2.13	HLH CR	1.110	7.81	1.97

F. *Energy Stored in High Angle Grain Boundaries*

The energy is stored not only in the sub-grain boundaries or sub-structures within ferrite grains but also in ferrite grain boundaries in this research. So, SE_{HAGB} values evaluated by Eq. 10 are listed in Table VI. Compared with the energy stored in sub-grain boundaries in ferrite matrix (Table III), the energy contributed from ferrite grain boundaries (Table VI) is much smaller, which is about 13% of the SE_d. This means that the sub-structures (i.e., cells and shear bands) within ferrite grains are the major sources for stored energy. Moreover, the SE_{HAGB} of steels with a combination of low coiling temperature and cold reduction holds a higher value.

Table VI SE_{HAGB} for hot band coils (HB) and cold rolled steels (CR)

Designation	SE_{HAGB} (HB) ($J\ cm^{-3}$)	SE_{HAGB} (CR) ($J\ cm^{-3}$)	Designation	SE_{HAGB} (HB) ($J\ cm^{-3}$)	SE_{HAGB} (CR) ($J\ cm^{-3}$)
LLL	0.21	0.50	LLH	0.16	0.33
LHL	0.25	0.47	LHH	0.18	0.27
MLL	0.26	0.51	MLH	0.17	0.33
MHL	0.22	0.43	MHH	0.19	0.25
HLL	0.22	0.46	HLH	0.18	0.30

V. Discussion

A. *The Comparisons in Stored Energy Evaluations Using the Three Methods*

This study compared three stored energy evaluation methods (sub-grain, IQ and KAM) for DP steels. The results demonstrated that both the sub-grain and KAM methods can quantitively estimate the stored energy, but in different ways, while the IQ method roughly indicated the trend of stored energy for steels with different initial pre-annealing conditions.

The comparisons in stored energy calculated by using sub-grain and KAM methods for DP hot band coils and cold rolled sheets are presented in Figs. 7 (a) and (b), respectively. In most cases, the stored energy values evaluated by the sub-grain method, but without the high angle grain boundary contribution, are higher than those calculated by the KAM method. For example, regarding sample LLL (0.04Al-0.06V-CT580ºC [853K]), the stored energy values, based on the sub grain and KAM methods, of its hot band coil are 1.65 $J\ cm^{-3}$ (Table III) and 1.01 $J\ cm^{-3}$ (Table IV), respectively. Similarly, in terms of its cold rolled sample, the stored energy calculated with the sub-grain method is about 1.19 $J\ cm^{-3}$ higher than that determined by the KAM method (Tables III and V).

After plastic deformation, the cold work is often manifested by forming dislocation structures such as deformation bands, cells [24] and cell walls. Similar to grain boundaries and twin boundaries, dislocation cell boundaries (also called sub-grain boundaries) originate from geometrically necessary dislocations, as proposed by Kuhlmann-Wilsdorf [43,44]. But, cell boundaries follow the low energy dislocation structures (LEDS) principle [43]. So, the

misorientations of cell boundaries are much smaller than those of grain boundaries and twin boundaries. In contrast, deformation bands and cell walls belong to incidental dislocation boundaries resulting from statistically mutual random trapping, often supplemented by "forest" dislocations [44]. In addition, most dislocations are placed in dislocation cell walls [45] and the misorientations of dislocation cell walls or shear bands are much smaller than those of cell boundaries. Calcagnotto et al.'s [31] work suggested that only the geometrically necessary dislocation densities could be calculated from KAM values, which means that energy stored in other dislocation structures such as deformation bands or cell walls cannot be obtained from the KAM method. This suggests that the KAM method is less accurate than the subgrain boundary method. So, SE_d (sub-grain) and SE_d (KAM) can be expressed by following Eqs. (14) and (15),

$$SE_d(\text{sub-grain}) = SE_{\text{deformation bands}} + SE_{\text{cells}} + SE_{\text{cell walls}} \text{ , while} \quad (14)$$

$$SE_d(\text{KAM}) = SE_{\text{cells}} \quad (15)$$

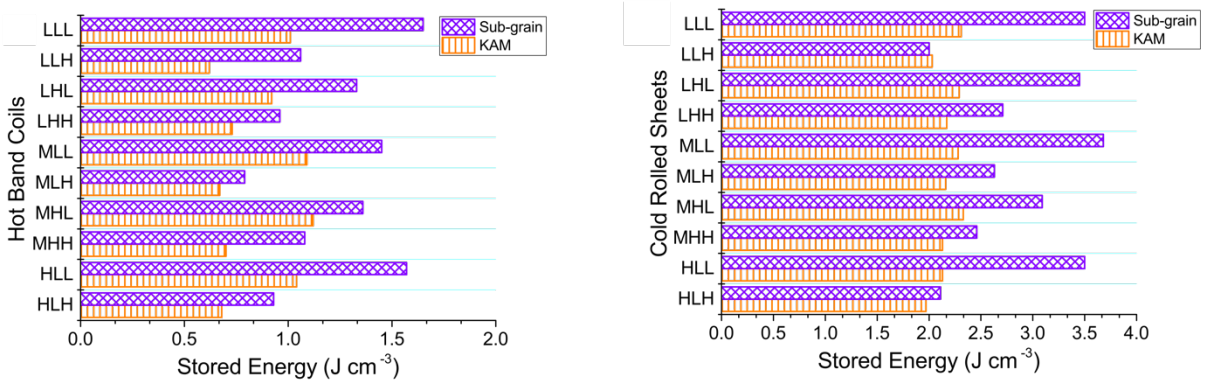

Figure 7-The stored energy values calculated by sub-grain and KAM methods for (a) hot band coils and (b) cold rolled sheet steels.

The difference between the two methods is due to the difference between equations (14) and (15), shown above.

B. *The Effects of Pre-Annealing Conditions on Stored Energy*

In this study, the stored energy of DP steels with several initial pre-annealing conditions were investigated. Fig. 8 shows the effect of coiling temperatures on stored energy calculated by the

sub-grain method for both DP hot band coils and cold rolled sheets. It is noticed that the stored energy values for steels with a low coiling temperature of 580ºC (853K) are higher than those for steels coiled at 677ºC (950K). The low temperature coiled steels are characterized by the existence of a larger volume fraction of acicular ferrite with high dislocation densities or more sub-structures, while the microstructures for steels coiled at 677ºC (950K) consist of polygonal ferrite with low dislocation densities [42]. The difference in dislocation densities of these two types of ferrite leads to the difference in stored energy values.

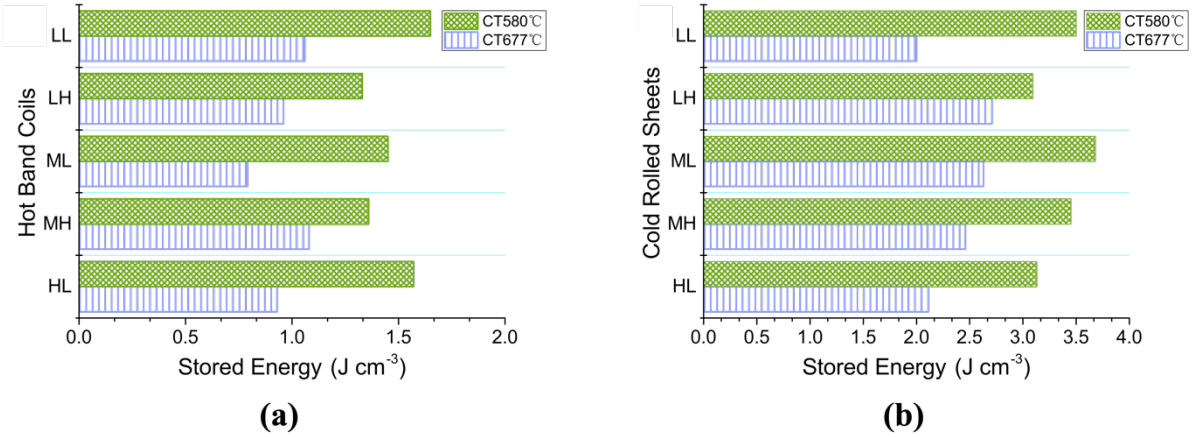

Figure 8-The stored energy evaluation based on sub-grain method for (a) hot band coils and (b) cold rolled sheet steels with two coiling temperatures

In addition to coiling temperatures, cold reductions also have a critical impact on stored energy. Fig. 9 presents the stored energy evaluation based on the sub-grain method for DP hot band coils (without cold work) and cold rolled sheets (60% cold work). It should be emphasized that the stored energy values of cold rolled sheets are higher than those of hot band coils with the same chemical compositions as well as coiling temperatures. In this case, after 60% cold rolling, cold work was consumed by forming numerous dislocation structures such as shear bands, cells [24] and cell walls and plastic strain energy was stored in the sub-grain boundaries within the ferrite matrix. It can be expected that the higher stored energy obtained from cold rolling increases the rates for ferrite recrystallization and austenite formation during intercritical annealing in the limited annealing time (~60 s) in the continuous galvanizing lines (CGL).

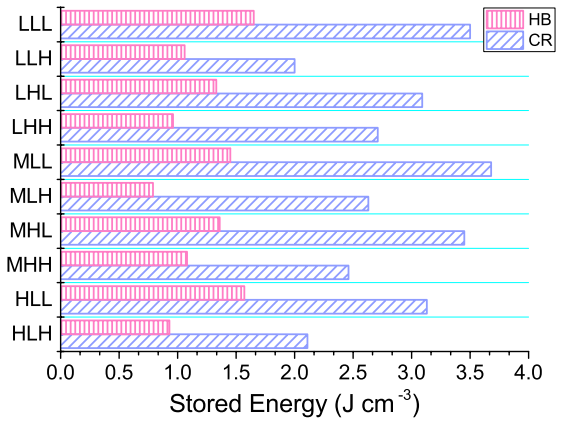

Figure 9-The stored energy evaluation based on sub-grain method for steels with and without 60% cold reduction

VI. CONCLUSIONS

The main purposes of this research were to compare three stored energy evaluation methods (sub-grain, IQ and KAM) for DP steels with different initial conditions, and to investigate the effects of pre-annealing conditions (i.e., coiling temperatures and cold reductions) on the stored energy. The findings can be summarized as follows.

(1) Both sub-grain and KAM approaches can predict the specific stored energy values for DP steels. Compared with the sub-grain method, the KAM method highly underestimates the stored energy, since only the energy stored in dislocation cells is considered in this approach. Regarding sub-grain method, all the dislocation structures (i.e., shear bands, cells and cells walls) are taken into consideration. Although IQ method cannot quantitatively predict the stored energy values, this method does help to show the trends of stored energy for steels with initial pre-annealing conditions.

(2) The minority of stored energy comes from HAGB energy, which accounts for about 13% of the energy stored in dislocation structures.

(3) The stored energy varies with both coiling temperatures and cold reductions. At a low coiling temperature, acicular ferrite nucleates and grows with high dislocation densities, while polygonal ferrite with low dislocation densities exists in the microstructures of steels coiled at a high

coiling temperature. The difference in dislocation density results in the difference in stored energy. In terms of cold reduction, the cold work is consumed by forming dislocation structures (shear bands, cells and cell walls), so the stored energy values of cold rolled sheets are always higher than those of hot band coils.

(4) The DP steels with the combination of low coiling temperature and cold reduction have the highest stored energy, providing more initial driving force for ferrite recovery and recrystallization as well as austenite nucleation and growth during following intercritical annealing.

REFERENCES

1 R.G. Davies: *Metall. Trans. A*, 1978, vol. 9, pp. 41–52.
2 C.C. Tasan, M. Diehl, D. Yan, M. Bechtold, F. Roters, L. Schemmann, C. Zheng, N. Peranio, D. Ponge, M. Koyama, K. Tsuzaki, and D. Raabe: *Annu. Rev. Mater. Res.*, 2015, vol. 45, pp. 391–431.
3 M.S. Rashid: *Annu. Rev. Mater. Sci.*, 1981, vol. 11, pp. 245–66.
4 O.A. Girina and N.M. Fonstein: in *Materials Science & Technology 2005*, 2005, pp. 65–76.
5 C.I. Garcia, K. Cho, K. Redkin, A.J. Deardo, S. Tan, M. Somani, and L.P. Karjalainen: *ISIJ Int.*, 2011, vol. 51, pp. 969–74.
6 C.I. Garcia, M. Hua, K. Cho, K. Redkin, and A.J. DeArdo: *Metall. Ital.*, 2012, vol. 104, pp. 3–8.
7 Y. Gong, J. Uusitalo, M. Hua, Y. Wu, and A.J. DeArdo: *J. Mater. Sci.*, 2019, vol. 54, pp. 7211–30.
8 Y. Wu and A.J. DeArdo: in *Materials Science and Technology 2018, MS and T 2018*, 2019.
9 F.L. Vogel, W.G. Pfann, H.E. Corey, and E.E. Thomas: *Phys. Rev.*, 1953, vol. 90, pp. 489–90.
10 W.. Hibbard and C.. Dunn: *Acta Metall.*, 1956, vol. 4, pp. 306–15.
11 J.S.L. Leach, E.G. Loewen, and M.B. Bever: *J. Appl. Phys.*, 1955, vol. 26, pp. 728–31.
12 1962.
13 T. Knudsen, W.Q. Cao, A. Godfrey, Q. Liu, and N. Hansen: *Metall. Mater. Trans. A*, 2008, vol. 39, pp. 430–40.
14 J. Lendvai, G. Honyek, A. Juhász, and I. Kovács: *Scr. Metall.*, 1985, vol. 19, pp. 943–6.
15 S.S. Hazra, A.A. Gazder, and E. V. Pereloma: *Mater. Sci. Eng. A*, 2009, vol. 524, pp. 158–67.
16 M.S. Paterson: *Philos. Mag.*, 1959, vol. 4, pp. 451–66.
17 G.R. Stibitz: *Phys. Rev.*, 1936, vol. 49, p. 862.
18 J.S. Kallend and Y.C. Huang: *Met. Sci.*, 1984, vol. 18, pp. 381–6.
19 N. Rajmohan, Y. Hayakawa, J.A. Szpunar, and J.H. Root: *Acta Mater.*, 1997, vol. 45, pp. 2485–94.
20 I.L. Dillamore, C.J.E. Smith, and T.W. Watson: *Met. Sci. J.*, 1967, vol. 1, pp. 49–54.
21 W.. Read and W. Shockley: *Phys. Rev.*, 1950, vol. 78, pp. 275–89.
22 W. Read: *Disloactaions in Crystals*, McGraw-Hill, 1953.
23 J. Tarasiuk, P. Gerber, B. Bacroix, and K. Piekos: *Mater. Sci. Forum*, 2002, vol. 408–412, pp. 395–400.
24 S.H. Choi and Y.S. Jin: *Mater. Sci. Eng. A*, 2004, vol. 371, pp. 149–59.
25 Y. Ateba Betanda, A.L. Helbert, F. Brisset, M.H. Mathon, T. Waeckerlé, and T. Baudin: *Mater. Sci. Eng. A*, 2014, vol. 614, pp. 193–8.
26 C. Fang, C.I. Garcia, S.H. Choi, and A.J. DeArdo: *Metall. Mater. Trans. A Phys. Metall. Mater. Sci.*, 2015, vol. 46, pp. 3635–45.
27 S.I. Wright and M.M. Nowell: *Microsc. Microanal.*, 2006, vol. 12, pp. 72–84.
28 S.I. Wright, M.M. Nowell, and D.P. Field: *Microsc. Microanal.*, 2011, vol. 17, pp. 316–29.
29 A.J. Wilkinson and T. Ben Britton: *Mater. Today*, 2012, vol. 15, pp. 366–76.
30 M.F. Ashby: *Philos. Mag.*, 1970, vol. 21, pp. 399–424.
31 M. Calcagnotto, D. Ponge, E. Demir, and D. Raabe: *Mater. Sci. Eng. A*, 2010, vol. 527, pp. 2738–46.

32 Y. Takayama and J.A. Szpunar: *Mater. Trans.*, 2004, vol. 45, pp. 2316–25.
33 F.J. Humphreys: *J. Mater. Sci.*, 2001, vol. 36, pp. 3833–54.
34 R.D. Doherty: in *Encyclopedia of Materials: Science and Technology*, Elsevier, 2001, pp. 7847–50.
35 J. Wu, P.J. Wray, C.I. Garcia, M. Hua, and A.J. DeArdo: *ISIJ Int.*, 2006, vol. 45, pp. 254–62.
36 D.A. Hughes, Q. Liu, D.C. Chrzan, and N. Hansen: *Acta Mater.*, 1997, vol. 45, pp. 105–12.
37 D.A. Hughes, N. Hansen, and D.J. Bammann: *Scr. Mater.*, 2003, vol. 48, pp. 147–53.
38 H. Gao and Y. Huang: *Scr. Mater.*, 2003, vol. 48, pp. 113–8.
39 W. Pantleon: *Scr. Mater.*, 2008, vol. 58, pp. 994–7.
40 H. Wawra: *Zeitschrift für Met.*, 1978, vol. 69, pp. 518–23.
41 E.E. Underwood: *Quantitative Microscopy*, McGraw-Hill, New York, 1968.
42 G. Krauss and S.W. Thompson: *ISIJ Int.*, 1995, vol. 35, pp. 937–45.
43 D. Kuhlmann-Wilsdorf: *Mater. Sci. Eng. A*, 1989, vol. 113, pp. 1–41.
44 D. Kuhlmann-Wilsdorf and N. Hansen: *Scr. Metall. Mater.*, 1991, vol. 25, pp. 1557–62.
45 H. Mughrabi: *Acta Metall.*, 1983, vol. 31, pp. 1367–79.